engineering proceedings

MDPI

Proceeding Paper

Continuous Localization-Assisted Collaborative RFI Detection Using the COTS GNSS Receivers †

Naveed Ahmed

Department of Engineering Cybernetics, Norwegian University of Science and Technology, 7034 Trondheim, Norway; naveed.ahmed@ntnu.no

† Presented at the European Navigation Conference 2023, Noordwijk, The Netherlands, 31 May–2 June 2023.

Abstract: Radiofrequency Interference (RFI) is a growing concern for many navigation-reliant applications. The dual benefits of RFI localization are considered: first, it can help with situational awareness by estimating the location of the interference source, and secondly, the results can be used to verify the detection of significant interference. The paper exploits the latter by proposing detection techniques making use of the localization results. The performance of the algorithms is evaluated using an experiment in a controlled lab environment where a wideband interference source is emulated in a UAV-based scenario. The detection results are validated using a reference detector operating in a non-position domain.

Keywords: RFI detection; carrier-to-noise density ratio (C/N_0); automatic gain control (AGC); minimum to second minimum error (MSME) ratio; majority voting

1. Introduction

The vulnerability of Global Navigation Satellite Subsystem (GNSS) signals due to their extremely low power that is often in the order of femtowatts has been widely known, and various disruptive events impacting the proper functioning of the receivers have been identified. The RFI can affect a receiver at different stages of its operation. An interference signal may attempt to target the pre-correlation stage, post-correlation stage or final position, velocity and time (PVT) computation of the receiver [1]. Therefore, it is important to identify where in the receiver chain the effect of the interference is observed. There has been a lot of work already conducted in the RFI detection domain, where research is more focused on the pre-correlation, post-correlation or hardware-based detection. The novelty in the work is introduced when the detection is studied starting from the fact that the localization, which often assumes the jamming has been pre-detected, could be used to determine whether the RFI source is actually presented. Hence, the localization results help to detect the presence of an interference source in an operating environment. AGC is a proven RFI detection tool that monitors the changes in the power level of the received signals [2,3]. Modern front-ends, which are usually equipped with a multi-bit analog-to-digital converter (ADC), can detect the interference by observing the histograms of the received samples. The drawbacks of such techniques are the sensitive nature of AGC itself and the need for careful received calibration. Pre-correlation detection techniques are implemented on the RF front-end output. The statistical assessment is performed on the received signals aiming to study the deviation in behavior indicating the presence of an interference [4]. The Finite Fourier Transform (FFT) properties are exploited to see the effect of interference on parameters like the FFT point and the test statistics mean and variance. In [5], detection is performed based on various parameters computed using the RF front-end output samples. The parameters computed in the paper include time domain energy, power spectral density (PSD), minimum detectable bias and the mean value estimator. A non-parametrical approach to detect interference is presented in [6],

check for updates

Citation: Ahmed, N. Continuous Localization-Assisted Collaborative RFI Detection Using the COTS GNSS Receivers. *Eng. Proc.* **2023**, *54*, 20. https://doi.org/10.3390/ENC2023-15441

Academic Editors: Tom Willems and Okko Bleeker

Published: 29 October 2023

Copyright: © 2023 by the authors. Licensee MDPI, Basel, Switzerland. This article is an open access article distributed under the terms and conditions of the Creative Commons Attribution (CC BY) license (https://creativecommons.org/licenses/by/4.0/).

where the authors studied the received signals using the Welch windowed periodogram. The technique is tested for both GPS L1 C/A and Galileo binary offset carrier (BOC(1,1)) signals. Such techniques are easily implemented on digital signal processing (DSP) or field-programmable gate array (FPGA) devices. The post-correlation family of detection techniques includes techniques that use the acquisition, tracking and navigation results for detection purposes. The pseudorange and C/N_0 are the parameters that appear to be most sensitive to the RFI [7]. A detection method using the position output monitoring is presented in [8]. It is observed that there is a deviation in the parameters pertaining to position accuracy such as C/N_0 and horizontal dilution of precision (HDOP), and large pseudorange errors were also noticed in the presence of interference.

In our work, we present two different RFI detection methods—the first uses the raw C/N_0 and AGC measurements obtained from nodes operating in a collaborative navigation scenario, whereas the second one uses the RFI localization results obtained using the method given in [9]. The first technique works on a principle of majority voting, where each participating node locally determines its detection state, and the final detection decision is made based on the collective detection flags. The second technique depends on the results obtained used a centralized approach for RFI localization. This approach defines a new detection metric that is mathematically represented as a minimum to second minimum position error (MSME) ratio. An experiment is conducted in a lab environment where an unmanned aerial vehicle (UAV)-based scenario is emulated and the UAVs follow a predefined trajectory in the presence of an interference source. The detection outcomes are compared with a reference detector designed using the receivers' observables in the non-position domain that, when considered together, indicate the overall jamming status.

The rest of the paper is organized as follows: Section 2 introduces different detection approaches in detail. Section 3 gives an insight of the experiments used to evaluate the detection algorithms. Section 4 discusses the results, and Section 5 concludes the paper.

2. RFI Detection Techniques

In this paper, we present post-correlation detection techniques and cover various detection approaches based on the jammer localization results discussed in [9]. The outcomes of the detection schemes are compared to a reference detector that is based on the receivers' parameters pertaining to their jamming detection capability.

2.1. Detection Using MSME Ratio Metric

It is crucial to have better localization results to utilize them for detection purposes. A better localization technique should have the least possible errors between estimated and real jammer positions. However, in certain marginal situations when the receivers become closer to entering or exiting the jamming zone of the jammer, this metric is not always a true indicator of jammer detection. A new metric is introduced that exploits the variability in localization results. In the current case, we are interested in observing the accuracy of the estimated jammer position. The metric is based on the ratio of the minimum position error to the second minimum position error. Considering the assumption of a ground-based jammer in our case, the MSME can be empirically defined for two-dimensional position errors. Based on relative MSME values, this metric can be used to identify both weak and strong interference zones. The MSME, γ_d, can be mathematically defined as

$$\gamma_d = \frac{\min(\Delta d)}{second\ \min(\Delta d)} \tag{1}$$

where Δd is the estimated position error. The γ_d is a dimensionless quantity and ranges from 0 to 1, with a lower value indicating the more erroneous estimation results that could either be due to presence of strong interference or some other reason such as poor geometry formed by nodes.

2.2. Majority Voting Detection Technique

The technique is based on the collective impact of the interference on the receivers' observables. A majority voting scheme is implemented on the instantaneous change in the C/N_0 and AGC. A jammer is potentially detected when the majority of the votes indicate the presence of jammer. Figure 1 shows the flow chart of how the scheme works for a system of N nodes. Based on the comparison of the instantaneous change in the C/N_0 with a defined threshold, the detection state is determined for each node individually. A majority voting is then implemented using the detection states obtained for all the nodes. The cycle then repeats for the observations from the next epoch.

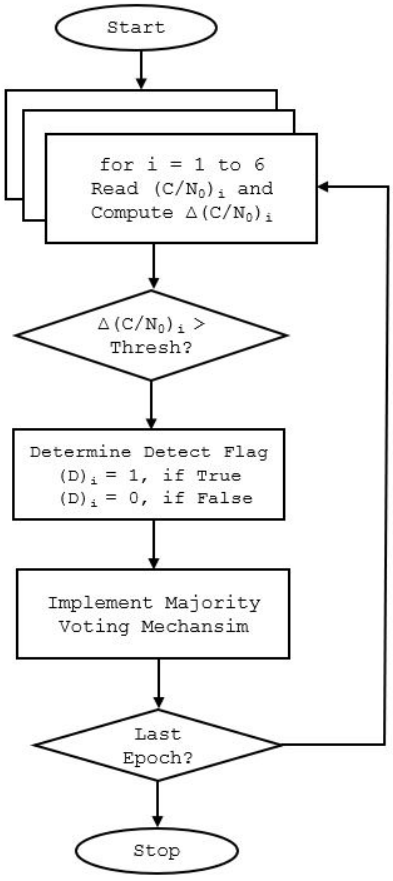

Figure 1. Majority voting scheme flow chart.

The threshold for comparison has been obtained based on the overall observation of C/N_0 degradation in the presence of interference.

Based on the observed jammer value in comparison to the threshold, an alert window is defined. Based on the length of the alert window, it is investigated how quickly the reference detection method, which is introduced in next section, is triggered. And considering the same C/N_0 degradation tolerance level, the robustness of the proposed detection method is determined.

2.3. Reference Detector Based on Receivers' Jamming Indicators

In order to evaluate the performance of the above two approaches, the results are compared with a reference detection approach. In our case, it is based on collective interpretation of the receivers' parameters pertaining to jamming detection. Table 1 shows some important parameters in the `UBX-MON-HW` message as defined in the u-Blox protocol specification document [10]. According to the document, the `jamInd` field only works for

narrowband interference (NBI) and continuous wave interference (CWI). Other values in the table should be studied together with the variation in C/N_0 or AGC.

Under normal situations, the AGC works on the thermal noise and hence the indicating factor, `agcCnt`, remains constant. Sometimes, it is mapped to the AGC voltages (0 to 3.3 V). In the case of RFI, the AGC reduces the RF gain to keep the signal within ADC dynamic range. Hence, the `agcCnt` value or AGC voltage decreases depending on the received signal strength of interference signals. The `noiseperMS` parameter gives the noise measured by the GPS core in dBm. `jamInd` is a CWI detection parameter, and its value lies on a scale from 0 to 255 and indicates the severity of the interference effect on the receiver. The `jammingstate` bits in the flag give information about the general performance of the receiver in the presence of interreference. A collective investigation of all such parameters helps in efficient detection.

Table 1. Jamming-related parameters in UBX-MON-HW receiver message.

Field Name	Field Description
agcCnt	AGC monitor (range 0 to 8191)
noisePerMS	Noise level as measured by the GPS core
jamInd	CW jamming indicator, scaled (0 = no CW jamming, 255 = strong CW jamming)
flags/JammingState	Output from jamming/interference monitor 0 = unknown or feature disabled; 1 = ok—no significant jamming; 2 = warning—interference visible but fix OK; 3 = critical—interference visible and no fix

3. Experiment Scenario Description

A network of six identical UAVs is deployed to fly over an open field of dimensions 2 km × 2 km. In the current context, an open field is considered that guarantees an open sky with clear reception of GNSS signals and offering no signal attenuation and blocking (multipath reflection due to urban canyon, foliage and so on), except due to interference. To ensure better observability during the scenario, the UAVs are programmed to fly at different altitudes following the predefined trajectory. For the sake of simplicity, no wind, jerk or other effects experienced by the UAVs have been considered in the article. Figure 2 shows UAVs and jammer trajectories in the scenario with a color bar representing the UAVs' ground speeds at various instants in the scenario that is also shown separately in Figure 3.

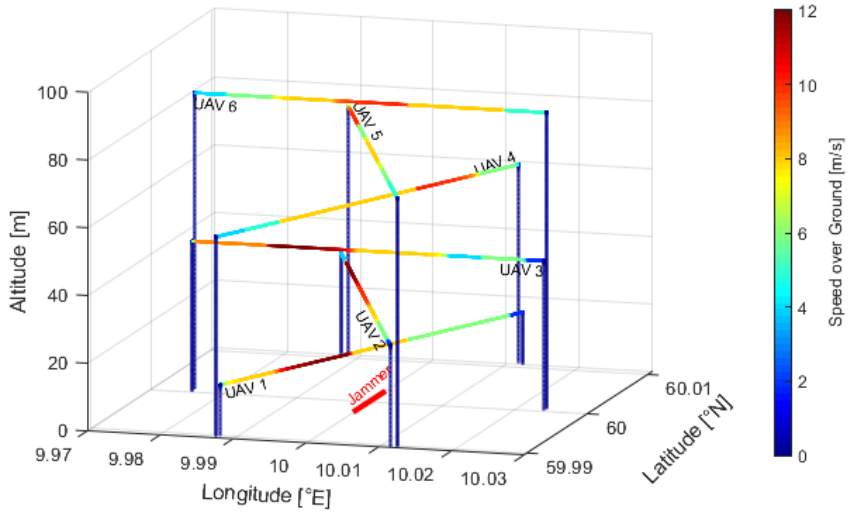

Figure 2. UAVs' and jammer's trajectories during the experiment in a 2 km × 2 km field.

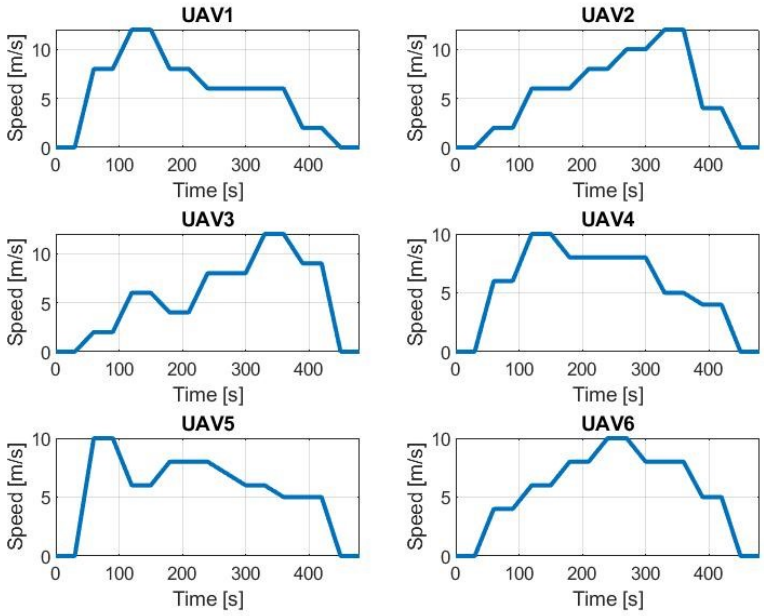

Figure 3. Simulated dynamics of the UAVs in the scenario.

3.1. Jammer Signals' Characteristics

We have considered wideband signal as our jamming signal of interest to study the impact of these signals on the C/N_0 and AGC of the receiver. Table 2 provides some important details about the simulated platform dynamics and other characteristics of the wideband interference signals. In the table, T_0 denotes the time at the start of simulation.

Table 2. Jammer's signal characteristics and dynamics simulated in the scenario.

Property	Value
Frequency (MHz)	−1575.42
Signal Power (dBm)	−60
Signal Bandwidth (MHz)	24
Speed (m/s)	2.5
Course over ground (deg)	0
ON time	(T_0 + 3 min) − (T_0 + 7 min)

3.2. Scenario Implementation

The aforementioned scenario is implemented on a Spirent HW GNSS simulator, and the interference signal is generated using the Spirent's Interference Signal Generator. The two signals are combined using an RF combiner, and the resulting results are given at the antenna input of the u-Box NEO-M8T GNSS receiver.

3.3. Brief Overview of RFI Localization

A centralized localization approach is followed, where it is assumed that all the cooperating nodes are capable of transmitting the distance from the jammer, calculated based on (2), to the central processing unit/node.

$$d_i = antilog_{10}\left(\frac{1}{10\alpha}\left(\frac{C_a}{N_0}\bigg|_{eff}^{i} - \bar{\beta}\right)\right) \quad (2)$$

where d_i is the distance of the ith UAV from the interference source, α is the path loss constant, C_a/N_0 is the effective average C/N_0 computed for the ith UAV and $\bar{\beta}$ is the

receiver specific constant that is obtained after calibration. Since we have six nodes (or UAVs in our case) in the system, we can formulate a system of six nonlinear equations that is solved using the iterative least squares estimation method. The unknown jammer coordinates can be given in the form of a state vector.

$$\mathbf{x} = \begin{bmatrix} x_j \\ y_j \\ z_j \end{bmatrix} \tag{3}$$

with a range measurement vector given as

$$\mathbf{y} = \begin{bmatrix} d_1 \\ d_2 \\ \dots \\ d_6 \end{bmatrix} \tag{4}$$

The relation between the change in the range and the change in the estimated state can be obtained by subtracting the predicted node to jammer measurement from the ranges obtained using (2) and applying first-order Taylor expansion.

$$\mathbf{\Delta y} = H\Delta\mathbf{x} \tag{5}$$

where H is the measurement or geometry matrix. The final solution can be obtained using the following:

$$\mathbf{\Delta\hat{x}} = (H^T H)^{-1} H^T \mathbf{\Delta y} \tag{6}$$

4. Results and Discussion

Figure 4 shows the estimated jammer positions obtained after collaborative RFI localization using C/N_0 and AGC [9]. The green boundary shows the region where the UAVs maneuver during the experiment. The quasistatic jammer's trajectory is represented by a red line. For the sake of analysis, the results within the 200 m $\times$ 200 m boundary are considered, shown with a magenta boundary.

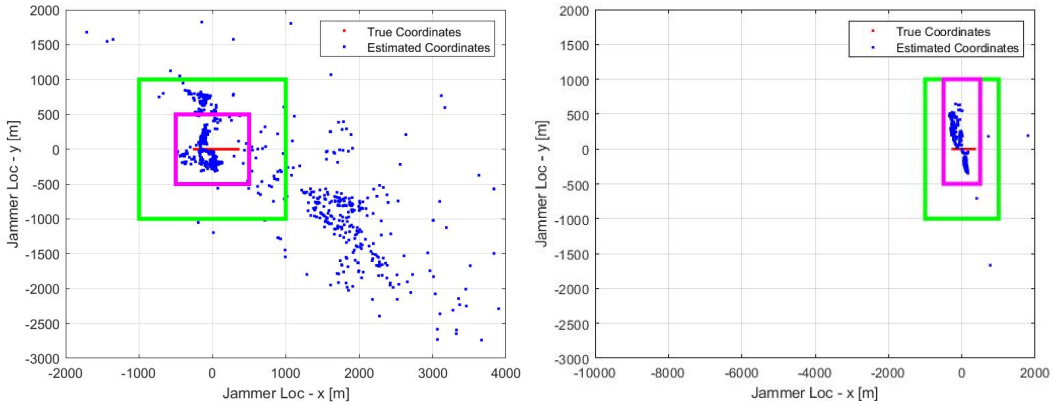

Figure 4. RFI localization results using C/N_0 (**top**) and AGC (**bottom**); area of UAVs' deployments zone is shown in green, whereas jammer detection region is shown in magenta—empirically selected based on the localization results.

4.1. MSME Results

Figure 5 shows the results of the MSME metric applied to the estimated position results. The figures show the variability in the localization results in terms of the ratio between the minimum to second minimum position error. The C/N_0 seems to be more sensitive compared to all other cases since the metric value goes to the least value, i.e., 0.955, which corresponds to a 4.5% variation in localization results, in contrast to 0.997 in the

case of AGC, which corresponds to 0.3%. Comparing the trend of metric values computed with C/N_0 with what was obtained using the AGC case, it seems that the former is more consistent at indicating the presence of interference since the variations happen in regular intervals during the jamming intervals and have the maximum effect when the interference source is turned ON and turned OFF, respectively.

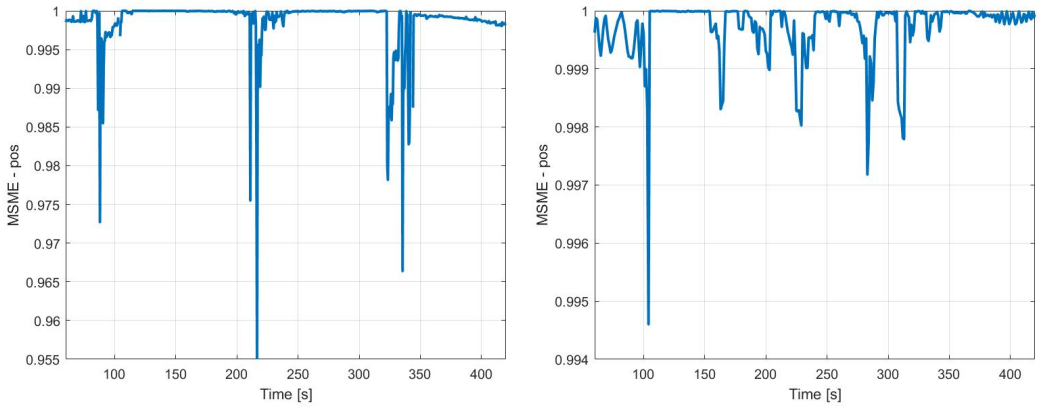

Figure 5. MSME results obtained using the localization results based on C/N_0 and AGC measurements.

4.2. Majority Voting Results

The majority voting approach has been implemented for a selected threshold using the method discussed in preceding sections. In the current case, the threshold is considered as 15 dB-Hz. Table 3 shows the final results for the detection technique based on the C/N_0 measurements. The technique is not fully adaptable for the case of AGC owing to its behavior and challenges in determining the threshold. The results from the table show that the RFI is collectively detected at the intervals between t = 210 s and t = 310 s. These are the instances when most or all the UAVs appear to be in closer proximity to the source. The level of contribution of each UAV in determining the overall decision can be determined through the state of each UAV, as given in different columns.

Table 3. Jammer signal characteristics and dynamics simulated in the scenario.

t[s]	Detection State—UAV1	Detection State—UAV2	Detection State—UAV3	Detection State—UAV4	Detection State—UAV5	Detection State—UAV6	Final Decision
200	1	1	0	1	1	0	1
205	1	0	0	1	1	0	0
210	1	1	0	1	1	0	1
215	1	1	0	1	1	1	1
220	1	1	0	1	1	1	1
225	1	1	0	1	1	1	1
230	1	1	0	1	1	1	1
235	1	1	1	1	1	1	1
240	1	1	1	1	1	1	1

Table 3. *Cont.*

t[s]	Detection State—UAV1	Detection State—UAV2	Detection State—UAV3	Detection State—UAV4	Detection State—UAV5	Detection State—UAV6	Final Decision
245	1	1	1	1	1	1	1
250	1	1	1	1	1	1	1
255	1	1	1	1	1	1	1
260	1	1	1	1	1	1	1
265	1	1	1	1	1	1	1
270	1	1	1	1	1	1	1
275	1	1	1	1	1	1	1
280	1	1	1	1	1	1	1
285	1	1	1	1	1	1	1
290	0	1	1	0	1	1	1
295	0	1	1	0	1	1	1
300	0	1	1	0	1	1	1
305	0	1	1	0	1	1	1
310	0	1	1	0	1	1	1
315	0	1	1	0	1	1	1
320	0	0	1	0	1	1	0
325	0	0	1	0	1	1	0
330	0	0	1	0	1	1	0
335	0	0	1	0	1	1	0
340	0	0	0	0	1	1	0
345	0	0	0	0	0	0	0
350	0	0	0	0	0	0	0
355	0	0	0	0	0	0	0
360	0	0	0	0	0	0	0
365	0	0	0	0	0	0	0
370	0	0	0	0	0	0	0
375	0	0	0	0	0	0	0
380	0	0	0	0	0	0	0
385	0	0	0	0	0	0	0
390	0	0	0	0	0	0	0
395	0	0	0	0	0	0	0
400	0	0	0	0	0	0	0

4.3. Reference Detection Approach Results

Figure 6 shows the plots of the parameters introduced in Table 1 obtained for the two UAVs closest to the jammer (UAV1 and UAV2) in the scenario (Figure 7 shows results for all the UAVs). The trends observed from the plots and the peculiar trend of variations indicate the presence of interference. However, the jamming severity could be declared as LOW based on the lower values of these jamming indication parameters. However, the important point is to obtain the temporal information of the interference injected into the scenario. This also serves as reference for comparing the results of other two techniques, as

we notice the detection results obtained using MSME metric and majority voting comply with the reference detection technique.

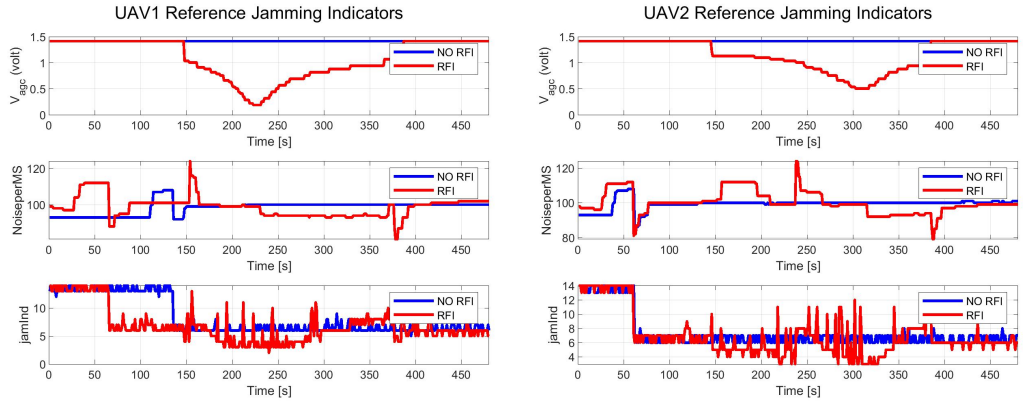

Figure 6. Reference jamming indicating parameters along with AGC voltage shown for UAV1 and UAV2, both in absence and presence of interference.

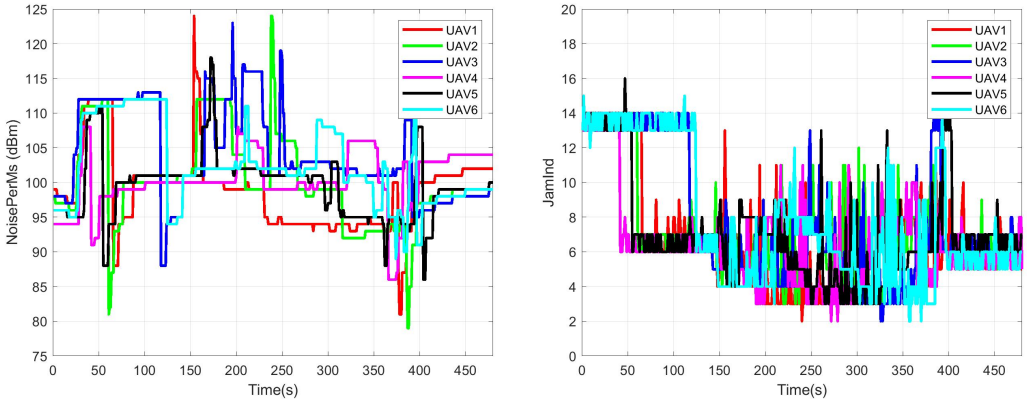

Figure 7. Comparison of NoisePerMs and JamInd values for different UAVs in the presence of interference.

5. Conclusions

The non-traditional methods of detecting interference have been presented in this paper. The variability in the localization results has been quantified using the MSME metric that proves to be instrumental in understanding detection. The majority voting technique detects interference based on the overall impact of the jammer on each node. The results are studied and presented in comparison with the reference techniques. The simulation results and observations show not only the potential of the discussed techniques to detect an RFI source but also to ensure that the localization results could possibly be used for detection. This is useful for situational awareness in practical situations and implementing a contingency plan.

Funding: This research received no external funding.

Institutional Review Board Statement: Not applicable.

Informed Consent Statement: Not applicable.

Data Availability Statement: Data sharing is not applicable to this article.

Conflicts of Interest: The author declares no conflict of interest.

References

1. Fabio, D. *GNSS Interference Threats and Countermeasures*; Artech House: Norwood, MA, USA, 2015.

2. Bastide, F.; Akos, D.; Macabiau, C.; Roturier, B. Automatic gain control (AGC) as an interference assessment tool. In Proceedings of the 16th International Technical Meeting of the Satellite Division of The Institute of Navigation (ION GPS/GNSS 2003), Portland, OR, USA, 9–12 September 2003; pp. 2042–2053.
3. Ndili, A.; Enge, P. GPS receiver autonomous interference detection. In Proceedings of the 1998 Position Location and Navigation Symposium, Palm Springs, CA, USA, 20–23 April 1996; pp. 123–130
4. Balaei, A.T.; Dempster, A.G. A statistical inference technique for GPS interference detection. *IEEE Trans. Aerosp. Electron. Syst.* **2009**, *45*, 1499–1511. [CrossRef]
5. Marti, L.; van Graas, F. Interference Detection by Means of the Software Defined Radio. In Proceedings of the 17th International Technical Meeting of the Satellite Division of The Institute of Navigation (ION GNSS 2004), Long Beach, CA, USA, 21–24 September 2004; pp. 99–109.
6. Tani, A.; Fantacci, R. Performance Evaluation of a Precorrelation Interference Detection Algorithm for the GNSS Based on Nonparametrical Spectral Estimation. *IEEE Syst. J.* **2008**, 2, 20–26. [CrossRef]
7. Groves, P.D. GPS Signal to Noise Measurement in Weak Signal and High Interference Environments. In Proceedings of the 18th International Technical Meeting of the Satellite Division of the Institute of Navigation (ION GNSS 2005), Long Beach, CA, USA, 13–16 September 2005; pp. 643–658.
8. Balaei, A.T.; Motella, B.; Dempster, A.G.; Rizos, C. Mutual Effects of Satellite Quality and Satellite Geometry on Positioning Quality. In Proceedings of the ION GNSS 2007 Conference, Fort Worth, TX, USA, 25–28 September 2007.
9. Ahmed, N.; Winter, A.; Sokolova, N. Low Cost Collaborative Jammer Localization Using a Network of UAVs. In Proceedings of the 2021 IEEE Aerospace Conference (50100), Big Sky, MT, USA, 6–13 March 2021; pp. 1–8.[CrossRef]
10. u-blox 8/u-blox M8 Recevier Description Including Protocol Specification. Available online: https://content.u-blox.com/sites/default/files/products/documents/u-blox8-M8_ReceiverDescrProtSpec_UBX-13003221.pdf (accessed on 23 March 2023).

Disclaimer/Publisher's Note: The statements, opinions and data contained in all publications are solely those of the individual author(s) and contributor(s) and not of MDPI and/or the editor(s). MDPI and/or the editor(s) disclaim responsibility for any injury to people or property resulting from any ideas, methods, instructions or products referred to in the content.